HHS Public Access

Author manuscript

Pain. Author manuscript; available in PMC 2019 May 01.

Published in final edited form as:

Pain. 2018 May ; 159(5): 968–977. doi:10.1097/j.pain.0000000000001171.

Neuroinflammation of the spinal cord and nerve roots in chronic radicular pain patients

Daniel Albrecht[1,2], **Shihab Ahmed**[3], **Norman Kettner**[4], **Ronald Borra**[5], **Julien Cohen-Adad**[6], **Hao Deng**[7], **Timothy Houle**[7], **Arissa Opalacz**[3], **Sarah Roth**[3], **Marcos Vidal Melo**[7], **Lucy Chen**[3], **Jianren Mao**[3], **Jacob Hooker**[1], **Marco L Loggia**[1,*], and **Yi Zhang**[3,*]

[1]A. A. Martinos Center for Biomedical Imaging, Department of Radiology, Massachusetts General Hospital, Harvard Medical School, Boston, MA, 02129 [2]Gordon Center for Medical Imaging, Department of Radiology, Massachusetts General Hospital, Harvard Medical School, Boston, MA, 02114 [3]MGH Translational Pain Research Center, Department of Anesthesia, Critical Care and Pain Medicine, Massachusetts General Hospital, Harvard Medical School, Boston MA 02114 [4]Department of Radiology, Logan University, Chesterfield, MO, 63017 [5]Medical Imaging Centre of Southwest Finland, Turku University Hospital, Turku, Finland; Department of Nuclear Medicine and Molecular Imaging, University of Groningen, University Medical Center Groningen, Groningen, Netherlands [6]Department of Electrical Engineering, Institute of Biomedical Engineering, Polytechnique Montreal, Montreal, Quebec, Canada; Functional Neuroimaging Unit, CRIUGM, Université de Montréal, Montreal, Quebec, Canada [7]Department of Anesthesia, Critical Care and Pain Medicine, Massachusetts General Hospital, Harvard Medical School, Boston MA 02114

Abstract

Numerous preclinical studies support the role of spinal neuroimmune activation in the pathogenesis of chronic pain, and targeting glia (e.g., microglia/astrocyte)- or macrophage-mediated neuroinflammatory responses effectively prevents or reverses the establishment of persistent nocifensive behaviors in laboratory animals. However, thus far the translation of those findings into novel treatments for clinical use has been hindered by the scarcity of data supporting the role of neuroinflammation in human pain. Here, we show that patients suffering from a common chronic pain disorder (lumbar radiculopathy), compared to healthy volunteers, exhibit elevated levels of the neuroinflammation marker 18kDa translocator protein (TSPO), in both the neuroforamina (containing dorsal root ganglion and nerve roots) and spinal cord. These elevations demonstrated a pattern of spatial specificity correlating with the patients' clinical presentation, as they were observed in the neuroforamen ipsilateral to the symptomatic leg (compared to both contralateral neuroforamen in the same patients as well as to healthy controls) and in the most caudal spinal cord segments, which are known to process sensory information from the lumbosacral nerve roots affected in these patients (compared to more superior segments).

Corresponding authors: Marco L. Loggia, PhD, Massachusetts General Hospital, A. A. Martinos Center for Biomedical Imaging, 149 Thirteenth Street, Room 2301, Charlestown, MA 02129, Phone: (617) 643-7267, marco@nmr.mgh.harvard.edu. Yi Zhang, MD, PhD, Massachusetts General Hospital, Center for Pain Medicine, 15 Parkman Street, Boston, MA 02114, Phone: (617) 726-8810, yzhang20@partners.org.

*Equal contribution, co-senior authors

Furthermore, the neuroforaminal TSPO signal was associated with responses to fluoroscopy-guided epidural steroid injections, supporting its role as an imaging marker of neuroinflammation, and highlighting the clinical significance of these observations. These results implicate immunoactivation at multiple levels of the nervous system as a potentially important and clinically relevant mechanism in human radicular pain, and suggest that therapies targeting immune cell activation may be beneficial for chronic pain patients.

INTRODUCTION

Chronic pain is a widespread public health issue, and its prevalence is enormous [32; 41]. Unfortunately, despite its great clinical and socioeconomic significance, our understanding of the pathophysiological mechanisms of chronic pain remains incomplete. As a result, currently available treatments (e.g., opioids) are unsatisfactory, as they are inefficacious in many patients, and are characterized by numerous side effects including abuse/misuse.

Substantial preclinical evidence has increased recognition of neuroimmune responses at multiple levels of the nervous system as an important contributor to the pathogenesis of persistent pain, including macrophage activation in the dorsal root ganglia [DRG; 22; 23], and activation of microglia and/or astrocytes in the spinal cord [10; 15; 19; 29; 37; 43; 48] and brain [24; 42]. Because activated macrophages and glial cells produce inflammatory mediators that activate or sensitize nociceptive neurons, the pharmacological inhibition of these cells can significantly reduce nocifensive behaviors in animals [14; 23; 30; 34; 47]. As such, the modulation of neuroimmune responses may represent a promising therapeutic strategy for pain disorders.

Among chronic pain disorders, lumbar radiculopathy is one of the most common. It presents clinically as low back pain radiating along the lower extremity (i.e., sciatica) along the dermatomes innervated by the affected spinal nerve roots. Lumbar radiculopathy can be caused by multiple etiologies including disc herniation, radiculitis, and lumbar spinal stenosis [6]. Despite the wealth of preclinical information, and knowledge that inflammation is associated with the initial acute phase of lumbar radicular pain [39], the role of neuroinflammation in chronic lumbar radiculopathy remains unknown. Clinically, the presumption of an inflammatory component to the pathophysiology of chronic sciatica, and specifically at the level of the nerve roots, provides a rationale for using anti-inflammatory epidural steroid injections (ESIs) as a treatment strategy for this disorder. However, this treatment demonstrates varying success [11], suggesting the presence of persistent nerve root inflammation in some patients, but not in others. Moreover, a recent study showed that a brief course of treatment with minocycline, which is thought to reduce central neuroinflammation, leads to some reductions in lumbar radicular pain [46], suggesting that glial modulation might be a viable treatment for at least some patients, as predicted by animal studies [19; 24; 31; 38; 45]. The development of clinical tests capable of detecting spinal nerve root as well as central neuroinflammation would have important clinical implications, including the possibility to guide patient selection for anti-inflammatory therapy targeting the peripheral (e.g., ESIs) or the central nervous system (e.g., glial modulators).

Here, we used simultaneous positron emission tomography / magnetic resonance (PET/MR) imaging and the radioligand [^{11}C]PBR28, which binds to the inflammatory marker 18kDa translocator protein (TSPO; formerly known as the peripheral benzodiazepine receptor) [2; 25; 26; 48], to test the hypothesis that lumbar radiculopathy is associated with immunoactivation at the level of both the intervertebral foramina (i.e., neuroforamina, which include dorsal root ganglion and nerve roots) and spinal cord. Furthermore, we hypothesized that patients demonstrating neuroforaminal inflammation would benefit most from an anti-inflammatory procedure targeting the neuroforamen, i.e., an ESI.

METHODS

Study design

This cross-sectional study was conducted at the Athinoula A. Martinos Center for Biomedical Imaging and the Translational Pain Research Center at Massachusetts General Hospital, Boston, MA. The protocol was approved by the Institutional Review Board and the Radioactive Drug Research Committee. The study was registered prior to subject recruitment at www.clinicaltrials.gov (Clinical Trials ID: NCT02130271). The manuscript is written in accordance with the STROBE checklist for observational studies.

Subjects

Between April 2014 and May 2016, we contacted 309 subjects. Of those contacted, we conducted phone screens on 110 subjects. 19 subjects with chronic lower extremity radicular pain lasting at least 3 months and 10 healthy control subjects underwent study procedures. Control subjects were recruited through advertising via flyers and printed announcements posted both within the MGH community and from the community at large, and pain patients were recruited via the abovementioned methods and through pools of pain patients under treatment at the MGH Center for Pain Medicine. Inclusion criteria for patients were: age between 18 and 75, diagnosis of lower extremity radicular pain with characteristic radiating pain in dermatomal distribution extending below the knee, and ongoing pain intensity of 4 or greater using the visual analog scale (VAS) during the week prior to enrollment. L4 dermatome pain was defined as presenting in the anterior thigh and medial leg. L5/S1 dermatome pain was defined as presenting in the posterolateral thigh and leg. All subjects were excluded for: recent hospitalization for a major psychiatric disorder, endorsing or testing positive for illicit drug use, chronic corticosteroid therapy, chronic opioid therapy, regular use of nonsteroidal anti-inflammatory (NSAIDs), recent lumbar epidural steroid injections (within 8 weeks), active cardiopulmonary disease, hepatic or renal insufficiency, any known inflammatory disease (e.g. inflammatory bowel disease), or any contraindications for PET or MR scanning (e.g. pregnancy, claustrophobia, ferromagnetic implants, etc.). Study procedures were fully explained to all subjects, and all subjects read and signed an informed consent document.

Screening visit

Each patient underwent a characterization session, which included a brief medical history and clinical examination by a board-certified pain management specialist (YZ, SA). The clinical examination determined the laterality of radicular pain (left or right leg), the

dermatome affected, duration of pain (years), current subjective pain level (Visual Analog Scale, anchored with 0="no pain" and 10="the most intense pain imaginable"), and response to prior epidural steroid injections (if any). Blood was collected to genotype subjects for the Ala147Thr *TSPO* polymorphism which is known to affect binding affinity for [^{11}C]PBR28 [21; 35]. Low-affinity binders (Thr/Thr; N = 2) were excluded from all analyses, whereas High- (Ala/Ala) or Mixed-affinity binders (Ala/Thr) were included. Urine was collected to test and exclude for recent illicit drug use.

PET/MR imaging

All simultaneous PET/MR imaging was performed on a 3T Siemens Biograph mMR system (Siemens Medical Solutions U.S.A., Inc., Malvern, PA, USA) with the radioligand [^{11}C]PBR28. [^{11}C]PBR28 binds to TSPO, a protein mostly expressed in the outer mitochondrial membrane. While TSPO is constitutively expressed by various cell types [7], it is commonly used as a marker of CNS inflammation because it is expressed at low levels in the healthy CNS, and it is dramatically upregulated in activated microglia and/or astrocytes in the context of neuroinflammation, including in response to spinal nerve injury [2; 25; 26; 48]. Additionally, TSPO is upregulated in activated macrophages [22], and therefore can also be used as a marker of peripheral inflammation. [^{11}C]PBR28 was produced in-house using a procedure modified from the literature [18].

MR imaging-related details

MRI data acquisition was performed using the body coil for transmit and a combination of the four-channel Body Matrix coils and the Spine Array Matrix for receive. Imaging focused on both the lumbar neuroforamina and lower thoracic spinal column. Anatomical images were collected using a combination of T1- and T2-weighted sequences. A T1-weighted (T1W) two-point Dixon 3D volumetric interpolated breath-hold examination (VIBE) sequence was acquired with the following parameters: parallel acquisition technique (PAT) GRAPPA factor 2, repetition time (TR) = 3.60s, echo time 1 (TE1) = 1.23ms, TE2 = 2.46ms, flip angle (FA) = 10°, slice thickness = 3.12mm, in-plane resolution = 4.1 × 2.6mm. The resulting images were segmented in-line to create a mu-map for MR-based attenuation correction (MRAC) of the PET data. MRAC scans were acquired immediately prior to initiation of PET scans. A high-resolution T1W axial anatomical turbo spin echo (TSE) sequence was acquired with the following parameters: TR = 2.69s, TE = 12ms, FA = 170°, matrix size = 256 × 179, slice thickness = 2mm, number of slices = 46, in-plane resolution = 1.0 × 0.7mm. This sequence was used for manual tracing of neuroforaminal regions of interest (ROIs). A T1W axial in-opposed phase gradient recoil echo (GRE) sequence was acquired with the following parameters: TR = 2.63s, TE = 3.83ms, FA = 65°, matrix size = 260 × 150, slice thickness = 2mm, number of slices = 76, in-plane resolution = 1.48 × 1.48mm. The field of view (FOV) was centered at the L4–L5 intervertebral disc. This sequence was used for visualization of overlaid PET signal. A high-resolution T2-weighted (T2W) sagittal anatomical TSE sequence was acquired with the following parameters: TR = 3.38s, TE = 109ms, FA = 150°, matrix size = 265 × 384, slice thickness = 2mm, number of slices = 30, in-plane resolution = 0.9 × 0.6mm, with the FOV centered at the L4–L5 intervertebral disc. This was used for registration of PET data and extracting PET signal.

PET acquisition

All subjects participated in a 90-minute dynamic acquisition, initiated with IV administration of [^{11}C]PBR28. Injected radioactivity (mean ± SD) was 392.6 ± 60 MBq for patients and 393.3 ± 57 MBq for controls (P = 0.97). Following the 90-minute lumbar neuroforamina PET scan, in a subset of willing participants (N = 9 patients, N = 9 controls) the PET FOV was shifted to image the lower thoracic spinal column, and an additional 20 minutes of dynamic PET data were then acquired in listmode format.

Data processing

For the neuroforaminal scan, a 30-minute static image was reconstructed from the 60–90 minute post-injection period. Images were reconstructed using 3D-OSEM and a 4-mm FWHM Gaussian kernel filter. Attenuation correction was performed using the MRAC-based mu-maps expanded using PET emission data and the maximum likelihood reconstruction of attenuation and activity (MLAA). PET images were converted from Bq/mL to standardized uptake value (SUV) maps by dividing all voxels by injected dose/body weight. SUV maps and high-resolution T1W images were imported into Osirix v. 3.9.4 (http://www.osirix-viewer.com) for defining regions of interest (ROIs) and extracting SUV. Fused PET/MR images were visually inspected to ensure the absence of motion artifacts. MR and PET images were well aligned for most subjects, but several patient and control PET scans required registration to MR data, which was manually performed using Osirix. On the T1W image, ROIs were manually traced on the left and right neuroforamina at the level of L3–L4, L4–L5, and L5–S1, the vertebral levels affected in the vast majority of lumbar radiculopathy patients. Neuroforamina definition was determined by anatomical boundaries: anterior - intervertebral disc/vertebrae; medial – thecal sac; posterior – apophyseal joint; lateral – psoas muscle. The structures contained in this area included the exiting spinal nerve roots, the corresponding DRG, and a cross section of the nerve root traversing to the lower adjacent level (Figure 1a). Determination of neuroforaminal ROIs was performed by a trained examiner and confirmed by an expert radiologist Average neuroforaminal SUV was extracted for each intervertebral level on axial sections, targeting the regions directly adjacent to intervertebral discs in order to minimize signal bleed from vertebrae. In addition, one subject's data was unusable due to attenuation artifacts and the inability to anatomically delineate the ROI, caused by a previous spinal fusion. There was no major pathological change impairing visualization of any neuroforaminal or spinal cord region for any other subjects. SUV ratio (SUVR) was calculated in patients by taking the ratio of SUV in target ROI (side ipsilateral to pain) to SUV in reference ROI (side contralateral to pain). In controls, SUVR was computed by taking the ratio of left to right SUV.

For the thoracic spinal PET data, a 20-minute static image was reconstructed from 90–110 minutes post-injection. Images were reconstructed and converted to SUV maps using the same procedure as for neuroforaminal data. Processing of the spinal cord images was performed with the recently developed Spinal Cord Toolbox [SCT; 13]. SCT enabled automated segmentation of whole spinal cord and labeling of vertebral levels from the high-res T2W image. As for the root data, MR and PET images of the spinal cord were well aligned for most subjects, but in a few subjects required coregistration, which was performed

using SCT. The spinal cord contained in T11–T12 vertebrae was chosen as a target region (Figure 1b), as the cord below and including T11 contains the lower lumbar/upper sacral spinal segments that receive nociceptive input from the sciatic nerve [40], and T11–T12 was present in all scanned participants (some participants had spinal cord termination above L1 due to natural interindividual variability). In one patient and two controls, the full extent of the cord contained in T12 was not present in the image, for these subjects the partial cord contained in T12 was included in the target region. Spinal cord contained in T7–T9 vertebrae was selected as a reference region, as these spinal segments are anatomically distant from those processing nociceptive input from the dermatomes affected in lumbar radiculopathy (Figure 1b). SUV was extracted from target and reference cord regions using the SCT. SUV ratio (SUVR) was calculated by taking the ratio of target ROI (cord contained in T11–T12) SUV to reference ROI (cord contained in T7–T9) SUV.

Epidural steroid injections

Lumbar epidural steroid injections were provided by patients' own treating physicians as part of their medical care. All epidural steroid injections were performed conforming to current standard of care with a fluoroscopic guided, para-median interlaminar approach on the side of pain symptoms and at the level of the involved nerve root (L4/5 level for L4 dermatomal pain and L5/S1 level of L5 or S1 dermatomal pain). A total volume of 4 ml (2 ml of 40 mg/ml triamcinolone and 2 ml of 0.25% bupivacaine) was administered after fluoroscopic confirmation of contrast dye spread in the epidural space. All injections were considered successful by their treating physicians and confirmed by contrast spread under fluoroscopy. Seven patients received ESIs after the PET/MR scan. Six of them received ESI treatments within 2 months after the scan. One subject received ESI treatment 8 months after the scan as the subject had medical insurance coverage in the interim. Two patients received ESIs 3–6 months prior to enrollment in the study but had no further ESIs up to two years after the scan. Therefore, we included these two patients with retrospective ESI treatment in the ESI response analysis. Subjective perception of percentage pain relief was documented at their follow up visits 4 weeks after the ESI treatment. For the two patients who received ESIs prior to enrollment, patients reported response to the prior ESI was documented at time of enrollment. Positive ESI response was defined as > 30% pain relief, negative response was defined as < 30% pain relief. The positive responders (N = 5) reported 90 ± 11% relief from ESI; all negative responders (N = 4) reported 0% relief from ESI.

Statistical analysis

Descriptive statistics were summarized for both continuous and categorical variables. Continuous variables were compared with t-tests. Based on the assumption that there should be no difference in PET signal between target and reference regions within healthy controls, we created an a priori derived grouping factor ("region"): "target" region in patients (neuroforamen analysis – neuroforamen ipsilateral to symptomatic leg in the affected dermatome; spinal cord analysis – cord contained in T11–T12 vertebrae), "reference" region in patients (neuroforamen analysis – neuroforamen contralateral to symptomatic leg in the affected dermatome; spinal cord analysis – cord contained in T7–T9) and healthy control region (neuroforamen analysis – left and right L5/S1 neuroforamen, as this was the affected dermatome in all but one pain patients; spinal cord analysis – cord contained in T7–T9 and

T11–T12). To account for repeated measures within an individual, we utilized a subject-level random intercept in mixed effects models while assessing the fixed effect regional differences in [^{11}C]PBR28 uptake in neuroforamen and spinal cord, controlling for *TSPO* genotype (high- or mixed-affinity binding status). Reference region in patients and mixed-affinity binding were included as reference terms within the mixed model. We hypothesized that genotype would differentially moderate regional differences in [^{11}C]PBR28 uptake, so we used ANOVA F statistics to test if adding a region × genotype interaction term would significantly increase the model fit from a model not including the interaction, as determined by Akaike Information Criterion (AIC [1]). If it was determined that addition of a region × genotype interaction improved the model fit, it was included in the model. Bonferroni-adjusted pairwise post-hoc comparisons were performed across regions (if applicable, at each level of genotype). Two initial post-hoc comparisons were planned, one comparing target region to reference region in patients, and one comparing target region in patients to healthy control regions. Supplementary linear regressions were also conducted to assess the effect of region and genotype on SUVR for both the spinal root and spinal cord analyses. Correlations between two continuous variables were estimated using linear regression. All statistical tests were two tailed with alpha set to 0.05. All analyses were performed with R statistical computing software (R, version 3.2.2; R Foundation for Statistical Computing, Vienna, Austria; Rstudio V1.0, Boston, MA).

RESULTS

Subjects

26 subjects (patients, n=16; controls, n=10) and 18 subjects (patients, n=9; controls, n=9) were included in the spinal root and spinal cord analyses, respectively. Patient and control characteristics for both analyses are listed separately in Table 1. There were no significant group differences in age, sex, *TSPO* genotype, injected dose, or BMI for either analysis ($p >$ 0.21).

Neuroforaminal immune activation in chronic lumbar radiculopathy

Using a mixed effects model, [^{11}C]PBR28 signal was compared across three anatomically-defined regions (grouping factor "region"): neuroforamen corresponding to pain symptoms in 16 patients (i.e., "target" region), neuroforamen contralateral to target region in patients (i.e., within-subject "reference" region), and corresponding neuroforamina in 10 healthy controls. We found that addition of a region × genotype interaction to the model significantly improved the fit ($F_{(48,46)} = 8.15$, $P = 0.0009$, ANOVA; AIC = −68.6), and thus was included in the final model. The model revealed that, for high-affinity binders only, the "target" neuroforaminal PET signal in patients was significantly elevated relative to both the signal from the "reference" side in the same individuals ($t_{(26)} = -4.10$, $P < 0.001$, corrected), as well as signal in healthy controls ($t_{(27.4)} = -3.09$, $P = 0.016$, corrected; Figure 2a,c, Table 2). In mixed affinity binders, "target" PET signal was not significantly different than "reference" side in the same patients ($t_{(26)} = -0.17$, $P = 0.99$, corrected), or in healthy controls ($t_{(27)} = 1.76$, $P = 0.36$, corrected; Figure 2a, Table 2). The absence of a significant regional effect in the mixed-affinity binders is likely due to the fact that a lower proportion of the PET signal in these participants reflects specific binding to TSPO [35]. See Figure 2b

and Table 3 for a complementary linear regression analysis using SUV ratio (SUVR; $F_{(3,22)} = 2.52$, $P = 0.08$, $R^2 = 0.26$).

Association between neuroforaminal [^{11}C]PBR28 signal and ESI-induced pain relief

A subset of patients (N=7) were treated with fluoroscopy-guided epidural steroid injections (ESIs) one week to several months after the imaging session. Two additional patients received ESIs more than two months prior to scanning. 5 patients (4 prospective and 1 retrospective ESI) reported 90 ± 11% relief from ESI (positive responders); 4 patients (3 prospective and 1 retrospective ESI) reported 0% relief from ESI (negative responders). We found that a positive response to ESI was observed only in patients with a ratio of target-to-reference SUV greater than 1 (i.e., target SUV > reference SUV; Figure 3). That is, a higher level of [^{11}C]PBR28 signal in the neuroforamen ipsilateral to pain, compared to the contralateral side, was associated with a positive response to ESI.

Spinal cord neuroinflammation in chronic lumbar radiculopathy

In order to determine whether radicular pain was also associated with spinal cord inflammation (i.e., glial activation), [^{11}C]PBR28 cord data was acquired in a subset of patients (N = 9) and controls (N = 9). Data were assessed with a mixed effects model between three regions: PET signal (SUV) from patients' cord contained in T11–T12 spinal segments ("target" region, which contains the spinal cord representations of the sciatic nerve), patients' T7–T9 signal (within-subject "reference" region), and the corresponding regions in controls. We found that target signal was significantly greater than both reference signal in patients as well as signal in healthy controls ($t_{(18)} = -4.82$, $P < 0.001$; $t_{(26.9)} = -3.6$, $P = 0.002$, respectively, corrected; Figure 4a, Table 4). See Figure 4b and Table 5 for a complementary related SUVR analysis ($F_{(2,15)} = 3.85$, $P = 0.04$, $R^2 = 0.34$). We did not observe significant associations between neuroforaminal and cord SUVR ($F_{(1,6)} = 0.21$, $P = 0.66$, $R^2 = 0.03$; Figure 5), between ESI response and spinal cord uptake ($P = 0.78$), or between central or peripheral PET metrics and pain ratings ($P = 0.23$ and 0.13, respectively).

DISCUSSION

We present here results supporting the occurrence of spinal neuroinflammation in patients with chronic radicular pain. Specifically, we show that patients demonstrate elevated TSPO levels, a putative marker of immune activation [2; 22; 25; 26; 48], in both nerve roots (ipsilateral to the symptomatic leg) and in the spinal cord (in spinal segments known to process sensory information from the legs). These findings, which extend and complement our earlier observations that TSPO levels are elevated in the brain of chronic low back pain patients [27], support the role of immunoactivation of the nerve roots as well as glial activation in the central nervous system as key components of the pathophysiology of chronic radicular pain. This is in line with a large body of preclinical data demonstrating neuroimmune activation as a result of peripheral nerve injury, both in the peripheral nervous system (e.g. DRG, nerve roots, [22; 23]) and central nervous system, including spinal cord [10; 14; 15; 34; 37; 43; 48] and brain [24; 42]. Previous studies have documented elevations in inflammatory mediators (e.g. pro-inflammation interleukins, prostaglandins, TNF-α, etc.) occurring in spinal tissue and CSF in individuals with disk disease, including herniation and

degeneration [39; 49]. This evidence indirectly suggests the involvement of neuroimmune modulation in these patients, as neuroimmune cells produce many of these molecules when activated during inflammation. More recently, studies using [^{18}F]FDG PET to assess metabolic activity showed increased binding in the spinal cord and compressed nerve roots of radicular pain patients [9; 50] and with increased aging [4], that was suggested to be related to inflammatory activity. While these studies are informative, the present experiment provides more direct insight into the role of neuroinflammation in lumbar radiculopathy, as it presents for the first time in-vivo evidence supporting elevated levels of a marker of immune activation.

Our findings suggest that immune responses in both central and peripheral nervous system may represent a promising therapeutic target. In the treatment of chronic sciatica pain, besides targeting spinal nerve roots with ESI as in current clinical practice, central immune activation may also need to be targeted for therapeutic intervention, as suggested by numerous preclinical studies [14; 19; 24; 30; 34; 37; 43; 48]. Large-scale studies are warranted to elucidate the relationship between these inflammatory signals and symptoms, as well as their viability as possible therapeutic targets and disease biomarkers. Once a definitive role for neuroinflammation in the pathology of sciatica has been confirmed in large-scale studies, it will be important to investigate surrogate techniques for identifying neuroinflammation that are more economic and do not include ionizing radiation for widespread use in a clinical setting. Integrated PET/MR imaging will likely be instrumental in the development of these surrogate strategies, because it allows a direct evaluation of the association between PET and MRI metrics simultaneously collected.

In our data, the ratio in [^{11}C]PBR28 signal between target and reference neuroforamen was associated with the response to ESI. These results suggest that variability in the magnitude of neuroforaminal inflammation may explain the large variability in responses to this treatment [11]. With validation in larger samples, our data suggest that pre-selecting patients based on the presence and/or magnitude of neuroforaminal inflammation might improve overall treatment response. It is important to note, however, that all but one of the patients who were positive responders also possessed a high-affinity binding *TSPO* genotype. While the effect of the Ala147Thr substitution in the *TSPO* gene on the binding affinity to second generation TSPO ligands is well known, the functional or clinical significance of this polymorphism is not well understood. One recent study did show that high-affinity binding status was associated with higher pain sensitivity in patients with fibromyalgia [20], suggesting that TSPO may play a role in modulating pain sensitivity, perhaps through its effects on neurosteroid production [12]. However, that association, along with the observations in the current dataset, will need to be validated with larger studies.

Study Limitations

Several additional caveats in the present study need to be mentioned. Analysis of PET data with an arterial input function and kinetic modeling is traditionally performed to quantify signal. However, there is a high amount of variability and complications associated with traditional modeling of TSPO PET data [44]. For this reason, SUV and SUVR metrics are

being increasingly used in TSPO PET analyses [3; 5; 8; 16; 17; 27; 28; 33; 36; 51], as we report here.

It is also important to acknowledge that the PET signal from both neuroforaminal and cord regions of interest is likely to include partial volume contribution from surrounding tissues (e.g., vertebrae), due to the coarse resolution of PET imaging (~4mm at center of field-of-view). However, the use of within-subject controls (the asymptomatic neuroforamen and the upper thoracic spinal cord segment) limits the impact of this concern, as both target and control regions should be similarly affected. In addition, there were no significant differences in the average PET signal in the vertebrae, or in size of target / reference regions of interest ($p > 0.10$, data not shown), giving us further confidence that the contamination from vertebral signal should not have significantly biased our results.

Another limitation of our study includes a relatively small sample size, particularly for the spinal cord data and the longitudinal component evaluating the association between neuroforamen TSPO uptake and ESI treatment response. Thus, further studies are needed to validate and expand upon these findings. Additionally, part of the treatment outcome data was collected retrospectively and thus is subject to patient recall bias. The time between the subjects PET/MRI scan and ESI treatment was not uniform, although this is unlikely to have affected the causality between PET findings and ESI response, as all patients had chronic lumbar radicular pain with stable pain symptoms.

While these caveats necessitate the use of caution when interpreting the results from our study, our preliminary observations are in line with previous preclinical literature supporting a role for neuroimmune activation in the establishment and/or maintenance of persistent pain conditions.

Acknowledgments

Drs. Loggia and Zhang are co-senior and co-corresponding authors. The study was supported by the following funding sources: 1R01NS095937-01A1 (M.L.), 1R21NS087472-01A1 (M.L.), NS082548-01A1 (Y.Z. and J.H.), 5T32EB13180 (T32 supporting D.A.). No authors report any conflicts of interest. We thank Grae Arabasz, Shirley Hsu and Regan Butterfield for their help with data acquisition.

References

1. Akaike, H. Breakthroughs in statistics. Springer; 1992. Information theory and an extension of the maximum likelihood principle; p. 610-624.
2. Albrecht DS, Granziera C, Hooker JM, Loggia ML. In vivo imaging of human neuroinflammation. ACS chemical neuroscience. 2016; 7(4):470–483. [PubMed: 26985861]
3. Albrecht DS, Normandin MD, Shcherbinin S, Wooten DW, Schwarz AJ, Zurcher NR, Barth VN, Guehl NJ, Johnson-Akeju O, Atassi N, Veronese M, Turkheimer F, Hooker JM, Loggia ML. Pseudo-reference regions for glial imaging with 11C-PBR28: investigation in two clinical cohorts. J Nucl Med. 2017
4. Aliyev A, Saboury B, Kwee TC, Torigian DA, Basu S, Wulff Christensen H, Alavi A. Age-related inflammatory changes in the spine as demonstrated by (18)F-FDG-PET:observation and insight into degenerative spinal changes. Hell J Nucl Med. 2012; 15(3):197–201. [PubMed: 23106050]
5. Alshikho MJ, Zurcher NR, Loggia ML, Cernasov P, Chonde DB, Izquierdo Garcia D, Yasek JE, Akeju O, Catana C, Rosen BR, Cudkowicz ME, Hooker JM, Atassi N. Glial activation colocalizes

with structural abnormalities in amyotrophic lateral sclerosis. Neurology. 2016; 87(24):2554–2561. [PubMed: 27837005]

6. Benzon, H., Rathmell, JP., Wu, CL., Turk, DC., Argoff, CE. Raj's practical management of pain. Elsevier Health Sciences; 2008.
7. Bribes E, Carriere D, Goubet C, Galiegue S, Casellas P, Simony-Lafontaine J. Immunohistochemical assessment of the peripheral benzodiazepine receptor in human tissues. J Histochem Cytochem. 2004; 52(1):19–28. [PubMed: 14688214]
8. Brody AL, Hubert R, Enoki R, Garcia LY, Mamoun MS, Okita K, London ED, Nurmi EL, Seaman LC, Mandelkern MA. Effect of Cigarette Smoking on a Marker for Neuroinflammation: A [11C]DAA1106 Positron Emission Tomography Study. Neuropsychopharmacology : official publication of the American College of Neuropsychopharmacology. 2017
9. Cipriano P, Yoon D, Gandhi H, Holley D, Thakur D, Ith M, Hargreaves B, Kennedy D, Smuck M, Cheng I, Biswal S. (18)F-FDG PET/MRI in Chronic Sciatica: Early Results Revealing Spinal and Non-spinal Abnormalities. J Nucl Med. 2017
10. Clark AK, Gentry C, Bradbury EJ, McMahon SB, Malcangio M. Role of spinal microglia in rat models of peripheral nerve injury and inflammation. European journal of pain. 2007; 11(2):223–230. [PubMed: 16545974]
11. Cohen SP, Bicket MC, Jamison D, Wilkinson I, Rathmell JP. Epidural steroids: a comprehensive, evidence-based review. Reg Anesth Pain Med. 2013; 38(3):175–200. [PubMed: 23598728]
12. Costa B, Pini S, Gabelloni P, Da Pozzo E, Abelli M, Lari L, Preve M, Lucacchini A, Cassano GB, Martini C. The spontaneous Ala147Thr amino acid substitution within the translocator protein influences pregnenolone production in lymphomonocytes of healthy individuals. Endocrinology. 2009; 150(12):5438–5445. [PubMed: 19846611]
13. De Leener B, Levy S, Dupont SM, Fonov VS, Stikov N, Louis Collins D, Callot V, Cohen-Adad J. SCT: Spinal Cord Toolbox, an open-source software for processing spinal cord MRI data. Neuroimage. 2017; 145(Pt A):24–43. [PubMed: 27720818]
14. Guo W, Wang H, Watanabe M, Shimizu K, Zou S, LaGraize SC, Wei F, Dubner R, Ren K. Glial-cytokine-neuronal interactions underlying the mechanisms of persistent pain. J Neurosci. 2007; 27(22):6006–6018. [PubMed: 17537972]
15. Hains BC, Waxman SG. Activated microglia contribute to the maintenance of chronic pain after spinal cord injury. J Neurosci. 2006; 26(16):4308–4317. [PubMed: 16624951]
16. Herranz E, Gianni C, Louapre C, Treaba CA, Govindarajan ST, Ouellette R, Loggia ML, Sloane JA, Madigan N, Izquierdo-Garcia D, Ward N, Mangeat G, Granberg T, Klawiter EC, Catana C, Hooker JM, Taylor N, Ionete C, Kinkel RP, Mainero C. Neuroinflammatory component of gray matter pathology in multiple sclerosis. Ann Neurol. 2016; 80(5):776–790. [PubMed: 27686563]
17. Hirvonen J, Kreisl WC, Fujita M, Dustin I, Khan O, Appel S, Zhang Y, Morse C, Pike VW, Innis RB, Theodore WH. Increased in vivo expression of an inflammatory marker in temporal lobe epilepsy. J Nucl Med. 2012; 53(2):234–240. [PubMed: 22238156]
18. Imaizumi M, Briard E, Zoghbi SS, Gourley JP, Hong J, Fujimura Y, Pike VW, Innis RB, Fujita M. Brain and whole-body imaging in nonhuman primates of [11C]PBR28, a promising PET radioligand for peripheral benzodiazepine receptors. Neuroimage. 2008; 39(3):1289–1298. [PubMed: 18024084]
19. Ji RR, Berta T, Nedergaard M. Glia and pain: is chronic pain a gliopathy? Pain. 2013; 154(Suppl 1):S10–28. [PubMed: 23792284]
20. Kosek E, Martinsen S, Gerdle B, Mannerkorpi K, Lofgren M, Bileviciute-Ljungar I, Fransson P, Schalling M, Ingvar M, Ernberg M, Jensen KB. The translocator protein gene is associated with symptom severity and cerebral pain processing in fibromyalgia. Brain Behav Immun. 2016; 58:218–227. [PubMed: 27448744]
21. Kreisl WC, Jenko KJ, Hines CS, Lyoo CH, Corona W, Morse CL, Zoghbi SS, Hyde T, Kleinman JE, Pike VW, McMahon FJ, Innis RB. Biomarkers Consortium PETRPT. A genetic polymorphism for translocator protein 18 kDa affects both in vitro and in vivo radioligand binding in human brain to this putative biomarker of neuroinflammation. J Cereb Blood Flow Metab. 2013; 33(1):53–58. [PubMed: 22968319]

22. Lacor P, Benavides J, Ferzaz B. Enhanced expression of the peripheral benzodiazepine receptor (PBR) and its endogenous ligand octadecaneuropeptide (ODN) in the regenerating adult rat sciatic nerve. Neurosci Lett. 1996; 220(1):61–65. [PubMed: 8977149]

23. Latremoliere A, Latini A, Andrews N, Cronin SJ, Fujita M, Gorska K, Hovius R, Romero C, Chuaiphichai S, Painter M, Miracca G, Babaniyi O, Remor AP, Duong K, Riva P, Barrett LB, Ferreiros N, Naylor A, Penninger JM, Tegeder I, Zhong J, Blagg J, Channon KM, Johnsson K, Costigan M, Woolf CJ. Reduction of Neuropathic and Inflammatory Pain through Inhibition of the Tetrahydrobiopterin Pathway. Neuron. 2015; 86(6):1393–1406. [PubMed: 26087165]

24. LeBlanc BW, Zerah ML, Kadasi LM, Chai N, Saab CY. Minocycline injection in the ventral posterolateral thalamus reverses microglial reactivity and thermal hyperalgesia secondary to sciatic neuropathy. Neurosci Lett. 2011; 498(2):138–142. [PubMed: 21571034]

25. Liu X, Li W, Dai L, Zhang T, Xia W, Liu H, Ma K, Xu J, Jin Y. Early repeated administration of progesterone improves the recovery of neuropathic pain and modulates spinal 18kDa-translocator protein (TSPO) expression. J Steroid Biochem Mol Biol. 2014; 143:130–140. [PubMed: 24607808]

26. Liu X, Liu H, Xu S, Tang Z, Xia W, Cheng Z, Li W, Jin Y. Spinal translocator protein alleviates chronic neuropathic pain behavior and modulates spinal astrocyte-neuronal function in rats with L5 spinal nerve ligation model. Pain. 2016; 157(1):103–116. [PubMed: 26307860]

27. Loggia ML, Chonde DB, Akeju O, Arabasz G, Catana C, Edwards RR, Hill E, Hsu S, Izquierdo-Garcia D, Ji RR, Riley M, Wasan AD, Zurcher NR, Albrecht DS, Vangel MG, Rosen BR, Napadow V, Hooker JM. Evidence for brain glial activation in chronic pain patients. Brain. 2015; 138(pt. 3):604–615. [PubMed: 25582579]

28. Lyoo CH, Ikawa M, Liow JS, Zoghbi SS, Morse CL, Pike VW, Fujita M, Innis RB, Kreisl WC. Cerebellum Can Serve As a Pseudo-Reference Region in Alzheimer Disease to Detect Neuroinflammation Measured with PET Radioligand Binding to Translocator Protein. J Nucl Med. 2015; 56(5):701–706. [PubMed: 25766898]

29. McMahon SB, La Russa F, Bennett DL. Crosstalk between the nociceptive and immune systems in host defence and disease. Nat Rev Neurosci. 2015; 16(7):389–402. [PubMed: 26087680]

30. Meller ST, Dykstra C, Grzybycki D, Murphy S, Gebhart GF. The possible role of glia in nociceptive processing and hyperalgesia in the spinal cord of the rat. Neuropharmacology. 1994; 33(11):1471–1478. [PubMed: 7532831]

31. Mika J. Modulation of microglia can attenuate neuropathic pain symptoms and enhance morphine effectiveness. Pharmacological reports : PR. 2008; 60(3):297–307. [PubMed: 18622054]

32. Nahin RL. Estimates of pain prevalence and severity in adults: United States, 2012. The journal of pain : official journal of the American Pain Society. 2015; 16(8):769–780. [PubMed: 26028573]

33. Nair A, Veronese M, Xu X, Curtis C, Turkheimer F, Howard R, Reeves S. Test-retest analysis of a non-invasive method of quantifying [(11)C]-PBR28 binding in Alzheimer's disease. EJNMMI Res. 2016; 6(1):72. [PubMed: 27678494]

34. Okada-Ogawa A, Suzuki I, Sessle BJ, Chiang CY, Salter MW, Dostrovsky JO, Tsuboi Y, Kondo M, Kitagawa J, Kobayashi A, Noma N, Imamura Y, Iwata K. Astroglia in medullary dorsal horn (trigeminal spinal subnucleus caudalis) are involved in trigeminal neuropathic pain mechanisms. J Neurosci. 2009; 29(36):11161–11171. [PubMed: 19741123]

35. Owen DR, Yeo AJ, Gunn RN, Song K, Wadsworth G, Lewis A, Rhodes C, Pulford DJ, Bennacef I, Parker CA, StJean PL, Cardon LR, Mooser VE, Matthews PM, Rabiner EA, Rubio JP. An 18-kDa translocator protein (TSPO) polymorphism explains differences in binding affinity of the PET radioligand PBR28. J Cereb Blood Flow Metab. 2012; 32(1):1–5. [PubMed: 22008728]

36. Paganoni S, Alshikho MJ, Zurcher NR, Cernasov P, Babu S, Loggia ML, Chan J, Chonde DB, Garcia DI, Catana C, Mainero C, Rosen BR, Cudkowicz ME, Hooker JM, Atassi N. Imaging of glia activation in people with primary lateral sclerosis. NeuroImage Clinical. 2018; 17:347–353. [PubMed: 29159046]

37. Raghavendra V, Rutkowski MD, DeLeo JA. The role of spinal neuroimmune activation in morphine tolerance/hyperalgesia in neuropathic and sham-operated rats. J Neurosci. 2002; 22(22): 9980–9989. [PubMed: 12427855]

38. Raghavendra V, Tanga F, DeLeo JA. Inhibition of microglial activation attenuates the development but not existing hypersensitivity in a rat model of neuropathy. J Pharmacol Exp Ther. 2003; 306(2):624–630. [PubMed: 12734393]
39. Saal JS, Franson RC, Dobrow R, Saal JA, White AH, Goldthwaite N. High levels of inflammatory phospholipase A2 activity in lumbar disc herniations. Spine (Phila Pa 1976). 1990; 15(7):674–678. [PubMed: 2218714]
40. Sayenko DG, Atkinson DA, Dy CJ, Gurley KM, Smith VL, Angeli C, Harkema SJ, Edgerton VR, Gerasimenko YP. Spinal segment-specific transcutaneous stimulation differentially shapes activation pattern among motor pools in humans. J Appl Physiol (1985). 2015; 118(11):1364–1374. [PubMed: 25814642]
41. Simon LS. Relieving pain in America: A blueprint for transforming prevention, care, education, and research. Journal of pain & palliative care pharmacotherapy. 2012; 26(2):197–198.
42. Taylor AM, Mehrabani S, Liu S, Taylor AJ, Cahill CM. Topography of microglial activation in sensory- and affect-related brain regions in chronic pain. J Neurosci Res. 2017; 95(6):1330–1335. [PubMed: 27574286]
43. Tsuda M, Shigemoto-Mogami Y, Koizumi S, Mizokoshi A, Kohsaka S, Salter MW, Inoue K. P2X4 receptors induced in spinal microglia gate tactile allodynia after nerve injury. Nature. 2003; 424(6950):778–783. [PubMed: 12917686]
44. Turkheimer FE, Rizzo G, Bloomfield PS, Howes O, Zanotti-Fregonara P, Bertoldo A, Veronese M. The methodology of TSPO imaging with positron emission tomography. Biochem Soc Trans. 2015; 43(4):586–592. [PubMed: 26551697]
45. Vanelderen P, Rouwette T, Kozicz T, Heylen R, Van Zundert J, Roubos EW, Vissers K. Effects of chronic administration of amitriptyline, gabapentin and minocycline on spinal brain-derived neurotrophic factor expression and neuropathic pain behavior in a rat chronic constriction injury model. Reg Anesth Pain Med. 2013; 38(2):124–130. [PubMed: 23337936]
46. Vanelderen P, Van Zundert J, Kozicz T, Puylaert M, De Vooght P, Mestrum R, Heylen R, Roubos E, Vissers K. Effect of minocycline on lumbar radicular neuropathic pain: a randomized, placebo-controlled, double-blind clinical trial with amitriptyline as a comparator. Anesthesiology. 2015; 122(2):399–406. [PubMed: 25373391]
47. Watkins LR, Martin D, Ulrich P, Tracey KJ, Maier SF. Evidence for the involvement of spinal cord glia in subcutaneous formalin induced hyperalgesia in the rat. Pain. 1997; 71(3):225–235. [PubMed: 9231865]
48. Wei XH, Wei X, Chen FY, Zang Y, Xin WJ, Pang RP, Chen Y, Wang J, Li YY, Shen KF, Zhou LJ, Liu XG. The upregulation of translocator protein (18 kDa) promotes recovery from neuropathic pain in rats. J Neurosci. 2013; 33(4):1540–1551. [PubMed: 23345228]
49. Wuertz K, Haglund L. Inflammatory mediators in intervertebral disk degeneration and discogenic pain. Global Spine J. 2013; 3(3):175–184. [PubMed: 24436868]
50. Zhou X, Cipriano P, Kim B, Dhatt H, Rosenberg J, Mittra E, Do B, Graves E, Biswal S. Detection of nociceptive-related metabolic activity in the spinal cord of low back pain patients using (18)F-FDG PET/CT. Scand J Pain. 2017; 15:53–57. [PubMed: 28850345]
51. Zurcher NR, Loggia ML, Lawson R, Chonde DB, Izquierdo-Garcia D, Yasek JE, Akeju O, Catana C, Rosen BR, Cudkowicz ME, Hooker JM, Atassi N. Increased in vivo glial activation in patients with amyotrophic lateral sclerosis: assessed with [(11)C]-PBR28. Neuroimage Clin. 2015; 7:409–414. [PubMed: 25685708]

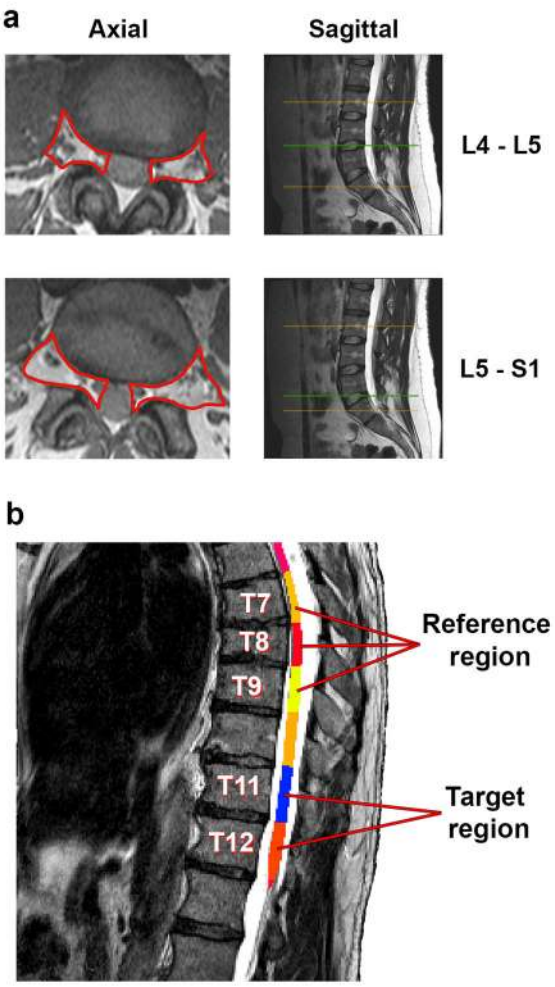

Figure 1. Visualization of spinal root and cord region of interest (ROI) placement

(**a**) Neuroforamina ROI labels. Right: Sagittal T2W images are shown to visualize the caudal/rostral level of ROI placement. Left: ROIs were manually drawn on the high-resolution T1W axial TSE sequence at the L3–L4, L4–L5, and L5–S1 levels (the latter two are pictured here). (**b**) Spinal cord ROI labels. Cord segments contained in T7, T8, and T9 served as the reference region segments contained in T11 and T12 were target regions, as this level of spinal cord receives nociceptive input from L4, L5, and S1 spinal roots.

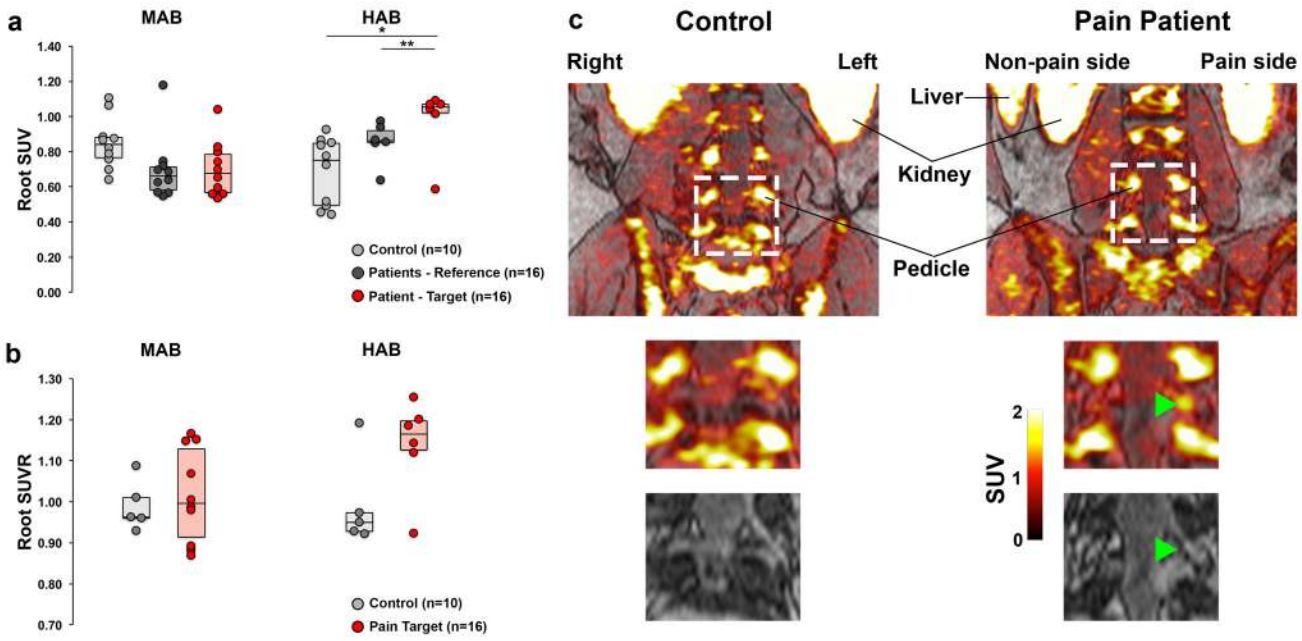

Figure 2.

Regional differences in spinal root [^{11}C]PBR28 signal. (**a**) A linear mixed effects model showed that high-affinity binding patients had elevated tracer uptake on the side ipsilateral to pain, relative to the side contralateral to pain and to uptake in healthy controls. Boxes represent 25% – 75% interquartile range, and horizontal line represents the median. *$t_{(27.4)}$ = −3.09, P = 0.016; ** $t_{(26)}$ = −4.10, P < 0.001, corrected. (**b**) Between group comparison of spinal root SUVR (patients – target divided by reference neuroforamina SUV; controls – left divided by right neuroforamina SUV). Statistical results from a linear regression analysis are shown in Table 3. (**c**) Individual lumbar PET/MR scans from two subjects, matched for age (control – 49; patient – 47), sex (M), and *TSPO* genotype (HAB). On the right (pain patient), focal elevation of [^{11}C]PBR28 uptake in the L4–L5 neuroforamen ipsilateral to the side of pain is highlighted by green arrowheads, compared to unaffected, contralateral side. This can be compared to the absence of neuroforaminal signal in the control subject's scan (left). The dashed boxes in the top panels are enlarged in the middle (PET overlaid on MR) and bottom (MR only) panels. Note: the coronal sections are shown only for display purposes; all data were extracted from axial slices.

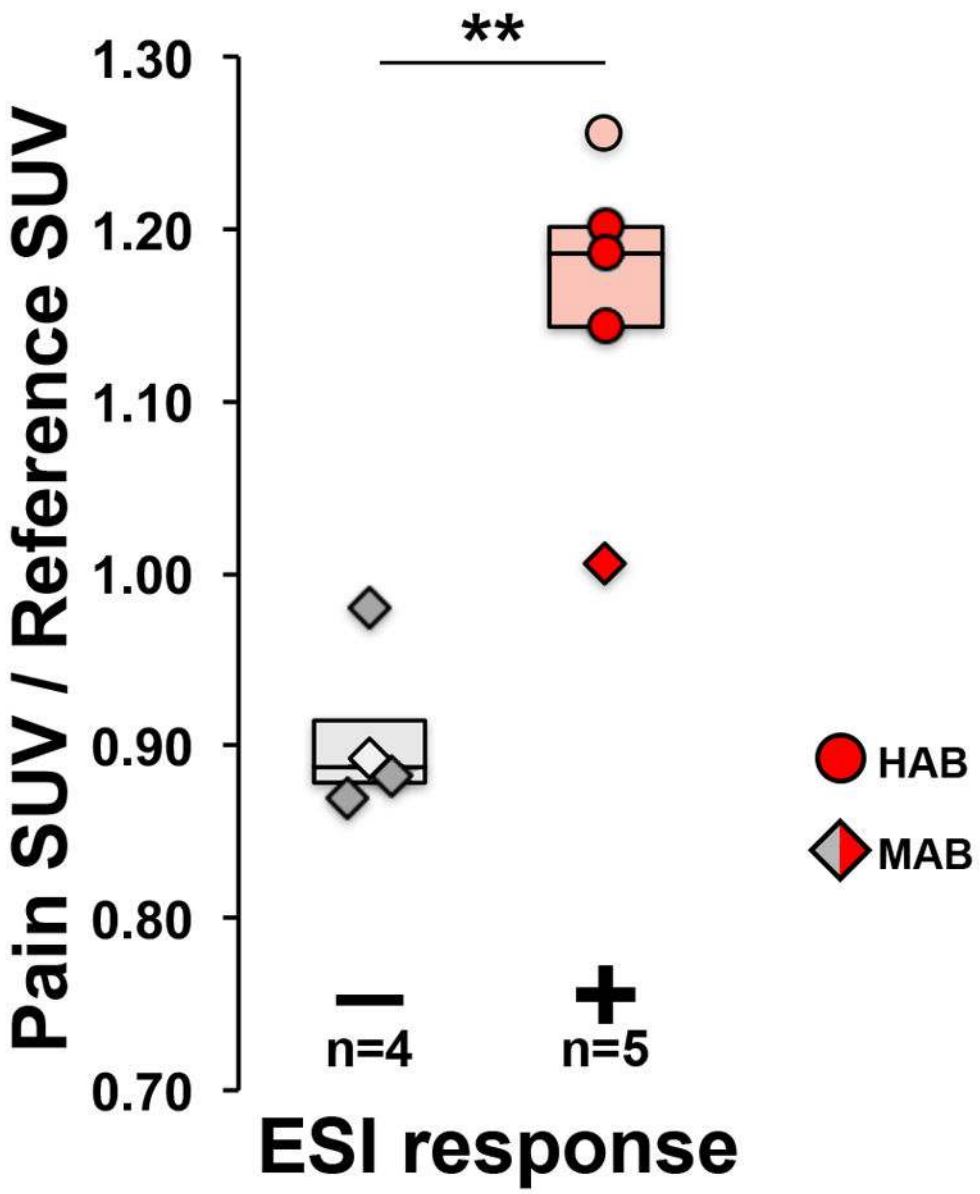

Figure 3.

Comparison between spinal root laterality (target SUV / reference SUV) in ESI non-responders (n=4; mean relief 0 ± 0%) and ESI responders (n=5; mean relief 90 ± 11%). ESI responders have a ratio of pain SUV to reference SUV greater than 1, indicating that increased lateral uptake in roots ipsilateral to pain is associated with a positive response to ESI. This is true both when using prospective data alone (i.e., patients receiving the ESI after the PET/MR scan) and also when including two retrospective subjects, $^{**}t_{(4.99)} = -3.94$, $P = 0.011$; and $t_{(6.27)} = -5.13$, $P = 0.002$, respectively, Welch two-sample t-test. HAB – high affinity binder; MAB – mixed-affinity binder. Light gray and light red identify a retrospectively-treated ESI non-responder and a responder, respectively.

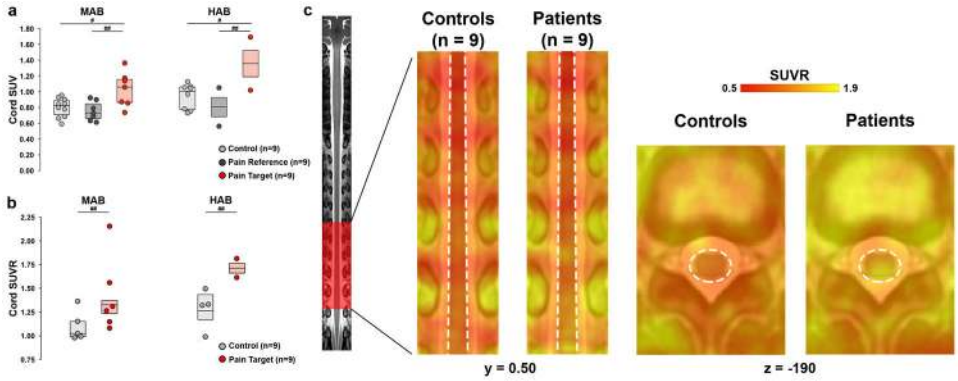

Figure 4.

Regional comparison of spinal cord [^{11}C]PBR28 uptake. (**a**) A linear mixed effects model showed that patients had elevated SUV in spinal cord contained in T11–T12 vertebrae, relative to spinal cord contained in T7–T9 vertebrae in patients and to uptake in healthy controls. Boxes represent 25% – 75% interquartile range, and horizontal line represents the median. While a genotype interaction term was not retained in this statistical model as it did not improve model fit, data from HAB and MAB subjects are presented separately here for illustrative purposes, and for consistency with Figure 2a. #differences between target signal in patients and signal in healthy controls (main effect, irrespective of genotype), $t_{(26.9)} = -3.6$, $P = 0.002$ (corrected); ##differences between target and reference in patients (irrespective of genotype), $t_{(18)} = -4.82$, $P < 0.001$ (corrected). (**b**) Between group comparisons of spinal cord SUVR (SUV from cord contained in T11–T12 divided by SUV from cord contained in T7–T9). See Table 5 for the results from a linear regression analysis. While a genotype interaction term was not retained in this statistical model, data from HAB and MAB subjects here are presented separately for illustrative purposes, and for consistency with Figure 2b. ##differences between patient and control SUVR (main effect, irrespective of genotype) at $P = 0.024$ (Table 5). (**c**) Mean spinal cord PET SUVR images for both controls and patients. Coronal and axial slices in the middle and right of the panel show [^{11}C]PBR28 data overlaid on the SCT T2 template. White dashed lines denote the borders of the spinal cord. A full-length image of the SCT T2 template on the left displays the spinal region common to all subjects (red overlay). The images shown here in SCT template space are for visualization purposes only, all data were extracted from images in subject space.

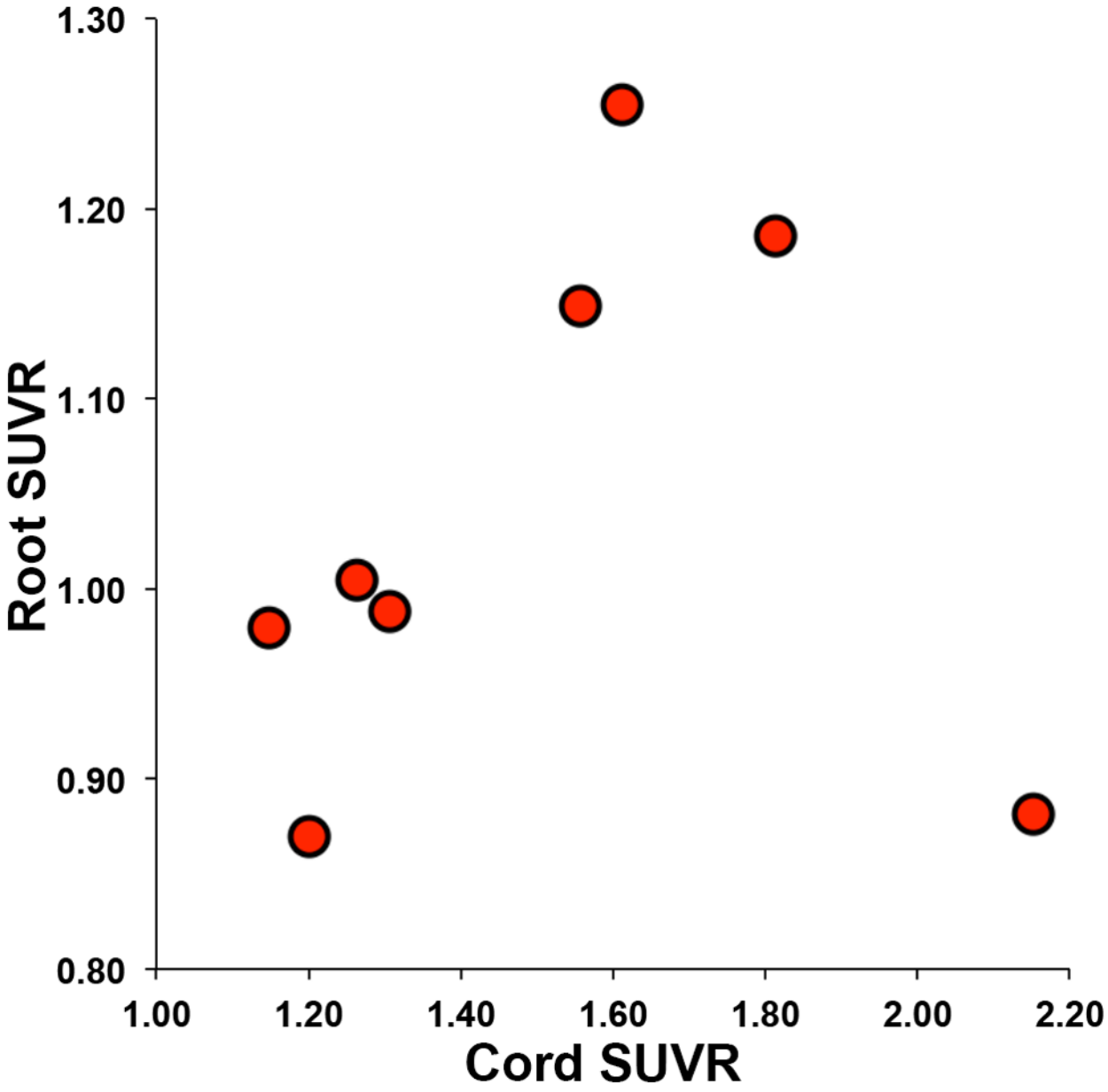

Figure 5. Relationship between spinal root and spinal cord SUVR

The association between spinal root and spinal cord SUVR was not significant with the inclusion of all pain patients for whom both root and spinal cord data were available (n=8). However, the regression became significant ($F_{(1,5)} = 17.13$, $P = 0.009$, $R^2 = 0.77$) after removal of one subject (bottom right). Notably, this subject did not receive any relief after ESI.

Table 1
Characteristics of pain patients enrolled in the study

Patient demographics and clinical characteristics. All continuous values are shown in mean ± SD. To differentiate subject subsamples from the spinal root and cord analyses, characteristics from each of the patient and control subgroups are displayed separately here. There were no significant group differences in any subject variables displayed here, for either spinal root or spinal cord analyses ($p > 0.21$).

Root analysis		
	Radicular pain patients (N = 16)	**Healthy controls (N = 10)**
Age (years)	51.2 ± 14	43.1 ± 19
Sex	6 F; 10 M	4 F; 6 M
TSPO Genotype	6 HAB; 10 MAB	4 HAB; 6 MAB
Injected Dose (mCi)	10.6 ± 1.6	11.0 ± 0.6
BMI	25.7 ± 2.8	27.1 ± 5.1
Location of Pain (Dermatome)	1 – L4; 15 – L5/S1	N/A
Location of Pain (Laterality)	8 – Left, 8 – Right	N/A
Pain Intensity (Visual analog score)	6.2 ± 1.5	N/A
Pain Duration (years)	5.6 ± 4.2	N/A
Spinal cord analysis		
	Radicular pain patients (N = 9)	Healthy controls (N = 9)
Age (years)	50.2 ± 9.0	42.4 ± 20
Sex	2 F; 7 M	3 F; 6 M
TSPO Genotype	2 HAB; 7 MAB	4 HAB; 5 MAB
Injected Dose (mCi)	10.5 ± 1.7	10.5 ± 2.1
BMI	24.1 ± 3.6	26.8 ± 5.2
Pain Intensity (Visual analog score)	6.17 ± 1.7	N/A
Pain Duration (years)	3.94 ± 2.2	N/A

Table 2

Linear mixed model statistics for spinal root SUV analysis

We included a region × genotype interaction term in the primary model that was retained in the final model as the addition of the interaction term was found to significantly improve the model fit. Bonferroni adjusted post-hoc comparisons compared mean outcomes at each level of genotype by region. Planned pairwise comparisons were between patient target and patient reference regions, and between patient target and healthy control regions. Reference side in patients for region and mixed-affinity binding for genotype were used as reference terms within the model. The mixed model showed significant interactions between *TSPO* genotype and neuroforamen SUV. Post-hoc testing revealed that this interaction was driven by significant increases in target SUV relative to reference SUV within patients as well as healthy control SUV in high-affinity binding individuals.

	Estimate	Std. Error	df	t-value	P-value	2.5 % CI	97.5 % CI
(Intercept)	0.697	0.05	29.1	13.942	<0.0001	0.595	0.798
Region							
Patients - reference	Reference						
Healthy controls	0.153	0.085	27.0	1.804	0.082	–0.019	0.326
Patients - target	0.004	0.024	26.0	0.171	0.866	–0.044	0.052
Genotype							
MAB	Reference						
HAB	0.157	0.082	29.1	1.926	0.064	–0.008	0.323
Region × genotype							
Patients - reference × HAB	Reference						
Healthy controls × HAB	–0.319	0.127	27.2	–2.515	0.018	–0.577	–0.061
Patients - target × HAB	0.121	0.039	26.0	3.133	0.004	0.043	0.2

Table 3
Linear regression results from spinal root SUVR analysis

This analysis did not replicate the significant differences in spinal root [^{11}C]PBR28 uptake seen with the regional linear mixed model ($F_{(3,22)} = 2.52$, $P = 0.08$, $R^2 = 0.26$; Figure 2a).

	Estimate	Std. Error	t-value	P-value
(Intercept)	0.990	0.048	20.7	1×10^{-14}
Group	0.025	0.059	0.428	0.673
Genotype	0.003	0.068	0.041	0.968
Group × Genotype interaction	0.120	0.087	1.375	0.183

Table 4

Linear mixed model statistics for spinal cord SUV analysis

A region × genotype interaction term was not retained in the final model as it was found to not significantly improve the model fit. Bonferroni adjusted pairwise post-hoc comparisons were proposed to compare mean outcomes at each region. SUV in spinal cord contained in T7–T9 vertebrae for region and mixed-affinity binding for genotype were used as reference terms within the model. There was a significant difference between reference T7–T9 SUV in patients and SUV in cord contained in T11–T12 in patients. There was also a significant effect of genotype.

	Estimate	Std. Error	df	t-value	P-value	2.5 % CI	97.5 % CI
(Intercept)	0.73	0.06	32.4	12.128	<0.0001	0.609	0.853
Region							
Patients - reference		Reference					
Healthy controls	0.062	0.076	26.9	0.812	0.424	−0.093	0.216
Patients - target	0.335	0.07	18.0	4.815	<0.0001	−2.238	0.479
Genotype							
MAB		Reference					
HAB	0.162	0.072	18.0	2.254	0.037	0.066	0.261

Table 5
Linear regression results from spinal cord SUVR analysis

The analysis replicated significant group differences in spinal cord SUVR (T11–T12 cord SUV normalized by T7–T9 cord SUV) between patient and control groups that were seen in SUV regional analysis ($F_{(2,15)} = 3.85$, $P = 0.04$, $R^2 = 0.34$; Figure 4a).

	Estimate	Std. Error	t-value	P-value
(Intercept)	1.08	0.110	9.82	1×10^{-6}
Group	0.331	0.131	2.52	0.024
Genotype	0.241	0.139	1.73	0.104